Particles I

Access the latest eBook →

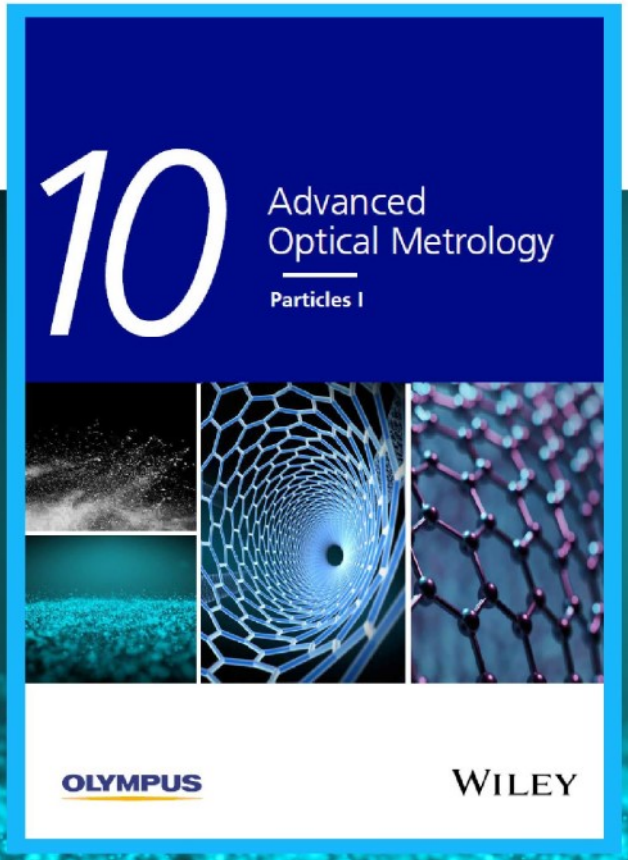

Particles: Unique Properties, Uncountable Applications

Read the latest eBook and better your knowledge with highlights from the recent studies on the design and characterization of micro- and nanoparticles for different application areas.

Access Now

This eBook is sponsored by

OLYMPUS

WILEY

small methods
www.small-methods.com

Unravelling the Complete Raman Response of Graphene Nanoribbons Discerning the Signature of Edge Passivation

Valeria Milotti, Claudia Berkmann, Jorge Laranjeira, Weili Cui, Kecheng Cao, Yifan Zhang, Ute Kaiser, Kazuhiro Yanagi, Manuel Melle-Franco, Lei Shi, Thomas Pichler,* and Paola Ayala**

Controlling the edge morphology and terminations of graphene nanoribbons (GNR) allows tailoring their electronic properties and boosts their application potential. One way of making such structures is encapsulating them inside single-walled carbon nanotubes. Despite the versatility of Raman spectroscopy to resolve strong spectral signals of these systems, discerning the response of long nanoribbons from that of any residual precursor remaining outside after synthesis has been so far elusive. Here, the terrylene dye is used as precursor to make long and ultra-narrow armchair-edged GNR inside nanotubes. The alignment and characteristic length of terrylene encapsulated parallel to the tube's axis facilitates the ribbon formation via polymerization, with high stability up to 750 °C when the hybrid system is kept in high vacuum. A high temperature annealing is used to remove the terrylene external molecules and a subtraction model based on the determination of a scaling factor related to the G-band response of the system is developed. This not only represents a critical step forward toward the analysis of the nanoribbon-nanotube system, but it is a study that enables unraveling the Raman signatures of the individual CH-modes (the signature of edge passivation) for GNR for the first time with unprecedented detail.

1. Introduction

The past three decades have set the ground for the incorporation of a variety of semiconducting nano-structures as fundamental building blocks in a wide range of technologies.[1–5] This implies finding mechanisms to model and control their structural performance tuning their electronic and optical properties. Semiconducting materials like graphene nanoribbons (GNR) are among the prime candidates for nanoelectronics.[6–8] These flat aromatic macromolecules arranged as narrow strips of graphene are defined by the number N of dimer–lines across their width. Their properties are determined by their edge structure (armchair or zigzag) and width[9, 10] but making GNR with atomically precise characteristics involves significant challenges.[11–13] Top-down methods struggle with edge quality and the control of the ribbon's width, while bottom-up

V. Milotti, C. Berkmann, W. Cui, T. Pichler, P. Ayala
Faculty of Physics
University of Vienna
1090 Vienna, Austria
E-mail: thomas.pichler@univie.ac.at; paola.ayala@univie.ac.at

J. Laranjeira
CICECO - Aveiro Institute of Materials
Department of Physics
University of Aveiro
Aveiro 3810-193, Portugal

M. Melle-Franco
CICECO - Aveiro Institute of Materials
Department of Chemistry
University of Aveiro
Aveiro 3810-193, Portugal

The ORCID identification number(s) for the author(s) of this article can be found under https://doi.org/10.1002/smtd.202200110.

DOI: 10.1002/smtd.202200110

Y. Zhang, L. Shi
State Key Laboratory of Optoelectronic Materials and Technologies
Nanotechnology Research Center
Guangzhou Key Laboratory of Flexible Electronic
Materials and Wearable Devices
School of Materials Science and Engineering
Sun Yat-sen University
Guangzhou 510275, China
E-mail: shilei26@mail.sysu.edu.cn

Y. Zhang
School of Engineering
Huzhou University
Huzhou, Zhejiang 313000, P. R. China

K. Cao
School of Physical Science and Technology
ShanghaiTech University
Shanghai 201210, China

U. Kaiser
Central Facility for Electron Microscopy
Electron Microscopy Group of Materials Science
Ulm University
89081 Ulm, Germany

K. Yanagi
Department of Physics
Tokyo Metropolitan University
Tokyo 192-039, Japan

approaches are in general more expensive and require complex precursor molecules or substrates for growth.[14] *On-surface* procedures require metal substrates—such as gold—to act both as catalyst and as edge control mechanisms.[15–20]

An alternative method for GNR-fabrication involves taking advantage of the chemically inert environment inside carbon nanotubes (CNT). This spatial constraint has been shown to be effective to confine and stabilize 1D structures such as inner concentric tubes,[21–23] carbyne chains,[24–27] and GNR with doped terminations.[28–30] Particularly, the availability and use of single-walled CNT (SWCNT) has two major advantages: the unidimensional spatial constraint and the protective role of the tube. For instance, GNR synthesized on a surface are quickly destroyed when inspected by Raman spectroscopy, while SWCNT stabilize the GNR structure preventing such radiation damage. Additionally, GNR can be tailored by choosing the diameter of the SWCNT[13, 31] and no transfer from a metallic substrate is needed to exclude any influence of the GNR's surrounding environment when they are inside a tube.[19] Small molecules such as coronene, fullerene derivatives,[28] ferrocene[31] and perylene,[29] have been successfully encapsulated and transformed into GNR inside SWCNT. Such hybrid systems offer the advantage to probe simultaneously the properties of a SWCNT and a semiconducting encapsulated GNR. The last mentioned encapsulated structure, perylene, is a short molecule that belongs to a family of dyes. It has been observed to stack at an angle in relation to the SWCNT's axis, which hinders its effective polymerization into GNR inside the tubes.[32] On the other hand, there are other dye molecules, such as terrylene or quaterrylene that offer a very similar aromatic configuration but differ in length. Both are longer than perylene and have an armchair configuration (See Figure S1, Supporting Information). In principle, using these longer molecules potentially increases the possibility to form long encapsulated ribbons. Although the control over the length of the GNR is an imperative need, it is not the only problem that needs to be solved for these systems. Discriminating the ribbon's properties from those of their precursor molecules is an unsolved issue in the characterization of GNR. Edge terminations are especially important in GNR, but the superposition of Raman-active modes from precursor molecules in the same range (never disentangled) has led to the absence of a detailed investigation into their Raman fingerprint. In this work, the terrylene dye molecule was used as precursor to make long and ultra-narrow (N = 5 C atoms width) armchair-edged GNR (5-AGNR) inside SWCNTs. These are semiconducting, with a predicted band-gap compatible with that of current semiconducting devices.[13,33,34] The alignment and the characteristic length of the terrylene molecules encapsulated parallel to the axis of the SWCNT have facilitated the 5-AGNR formation, with a high ribbon's stability when annealed up to 750 °C and the hybrid system is kept in high vacuum. Long and very narrow GNR inside nanotubes of 1.4 nm in diameter have been revealed by transmission electron microscopy (TEM). Furthermore, to obtain a clean hybrid, a high temperature annealing in vacuum has been successfully used to remove unfilled precursors without damaging the encapsulated polymerized 5-AGNR. Critical parameters have been established by examining the decreasing contamination as a function of the heating temperature and with this preliminary procedure, an empirical model

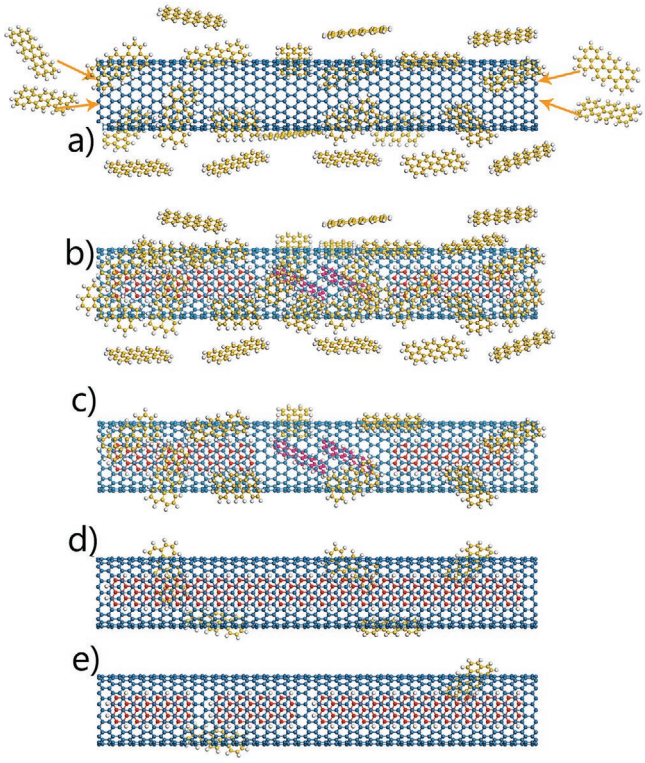

Figure 1. Formation process of 5-AGNR@SWCNTs: a) filling of the SWCNTs with terrylene at 350 °C, b) partial polymerization without further treatment, c) 5-AGNR@SWCNTs after washing, d) washed hybrids with further annealing up to 600 °C, and e) annealed hybrids above 600 °C where only traces of outer terrylene can be found.

supported by density functional theory (DFT) was developed to discern the signal of the traces of terrylene outside the hybrids from that arising from the spectra of the inner GNR terminated by H atoms. This allowed us to unravel the Raman signatures of the individual CH-modes for GNR with unprecedented detail.

2. Results and Discussion

SWCNTs (buckypapers) were filled with terrylene at 350 °C as sketched in **Figure 1**a. A partial polymerization of the terrylene into short ribbons occurs (Figure 1b) without further thermal treatment. This material was examined *as-synthesized* by Raman spectroscopy. Since molecules from non-polymerized terrylene can be expected to remain outside of the nanotube after the encapsulation process, as reported for other fillers,[29] it is inferable that large amounts of non-encapsulated terrylene can interfere with the Raman signal of the newly formed hybrid structures. The first approach to improve the sample cleanliness was to wash the hybrids (sketched in Figure 1c) with dichloromethane (DCM). Raman spectra were acquired before and after washing. Figure S2, Supporting Information, shows that the background fluorescence clearly disappeared after rinsing. This also enabled a better visualization of the material by means of TEM. The high resolution micrograph obtained in an aberration corrected system (**Figure 2**a) shows long and broad structures inside a hollow tube. The filling can be confirmed by the contrast profile in Figure 2b based on

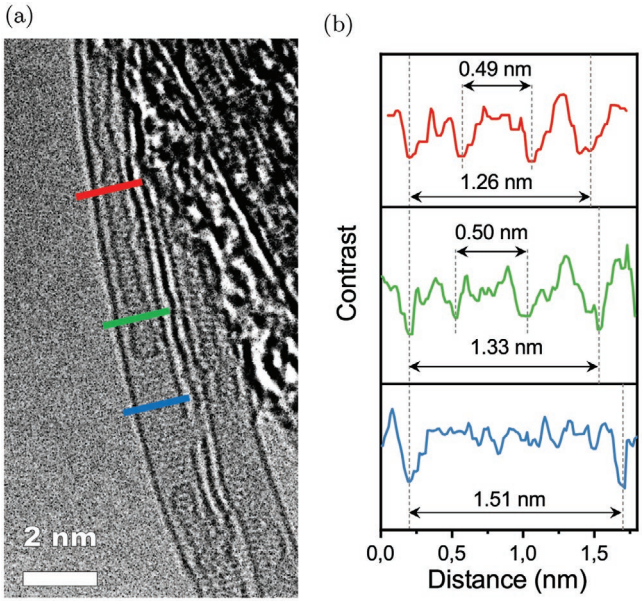

Figure 2. a) High resolution TEM micrograph of 5-AGNR@SWCNTs. b) Contrast profile along the lines highlighted in the left side panel.

the cross sections selected randomly with the color lines on the left-side panel. The theoretical width of a freestanding 5-AGNR is 0.49 nm, which is very close to the value estimated from the width profile in the top two panels in Figure 2b. Additional TEM micrographs can be found in Figure S3, Supporting Information.

2.1. Identification of the CH-Vibration Signatures

The subsequent analysis primarily focuses on revealing the signature of the CH-modes based on understanding the Raman spectral features observed for terrylene, pristine nanotubes, and the encapsulated ribbons.[20,35] The three bottom spectra in **Figure 3**a correspond to the Raman signals recorded using a 785 nm excitation wavelength. Using this laser line it is possible to see a broader active response (more peaks) and it can clearly be seen that the spectrum of the filled structure is not a simple overlap of the first two, but it is composed by additional features that could be associated to the formation of nanoribbons. Furthermore, when the 785 nm excitation wavelength is used to measure terrylene, given that the excitation energy is below its optical band gap, the fluorescence background is low. In this way, the corresponding Raman spectrum of crystalline terrylene can be safely used as reference (see Figure S6, Supporting Information). Given the molecular structure of terrylene, the most probable configuration for the encapsulated ribbons is 5-AGNR, as mentioned above. Therefore, the 5-AGNR inside the SWCNT (5-AGNR@SWCNT) is taken as starting point for the next step, which was a multi-frequency Raman analysis with the following laser wavelengths: 568 nm (because this is close to the terrylene optical band gap), 633 nm (in resonance with the encapsulating SWCNT), and 785 nm (close to the predicted GNR band gap). With these considerations, several features can be identified and ascribed to each structure. To start, the signal around ≈1570 cm^{-1} corresponds to the G-band, which has a contribution from the SWCNT and

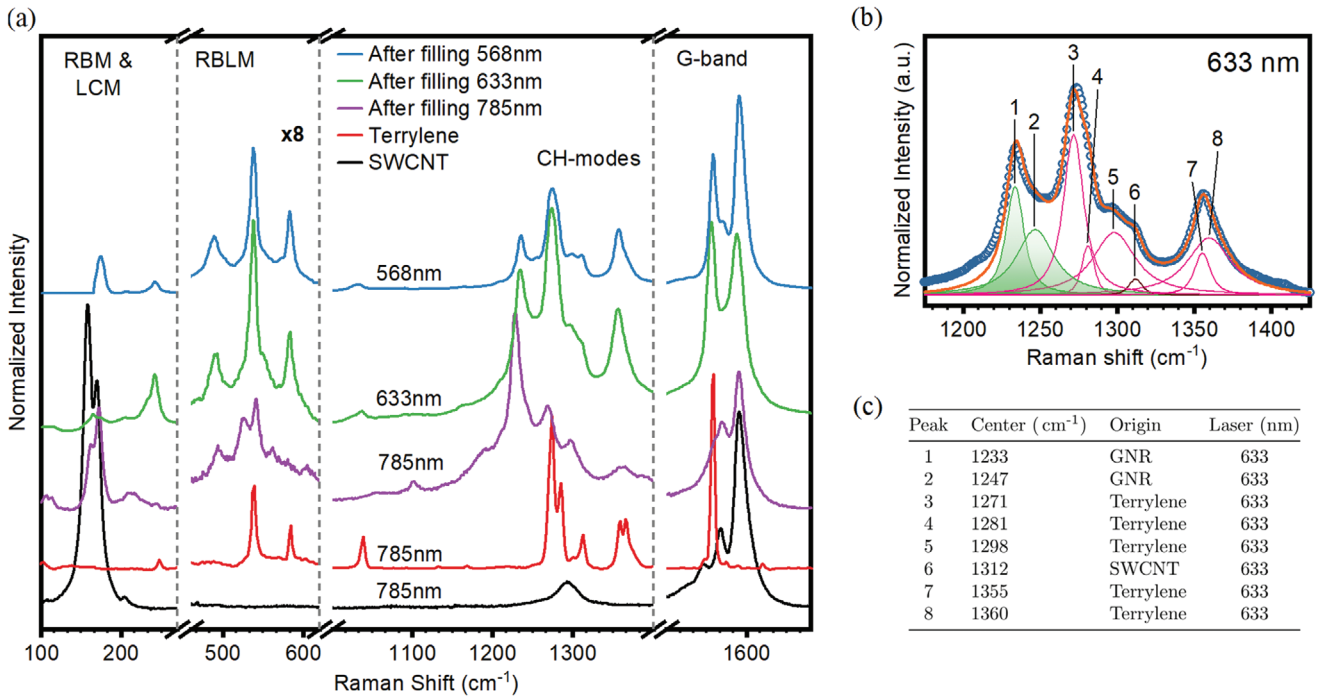

(c)

Peak	Center (cm^{-1})	Origin	Laser (nm)
1	1233	GNR	633
2	1247	GNR	633
3	1271	Terrylene	633
4	1281	Terrylene	633
5	1298	Terrylene	633
6	1312	SWCNT	633
7	1355	Terrylene	633
8	1360	Terrylene	633

Figure 3. a) From bottom to top: Raman spectra of pristine SWCNT and van der Waals crystalline terrylene powder acquired with a 785 nm, excitation wavelength. Terrylene filled SWCNT at 350 °C and subsequently washed with DCM were inspected by a multi-frequency Raman analysis. Plotted above are the spectra acquired with the 785, 633, and 568 nm excitation wavelengths, which are normalized to the G-band. b) Spectral deconvolution of the CH-modes obtained with an 633 nm excitation wavelength on a sample right after filling without further high temperature treatment. The identified components correspond to terrylene or SWCNT. Additional components can correspond to GNR vibrations (explained further in the text). c) Centers of peaks identified in (b).

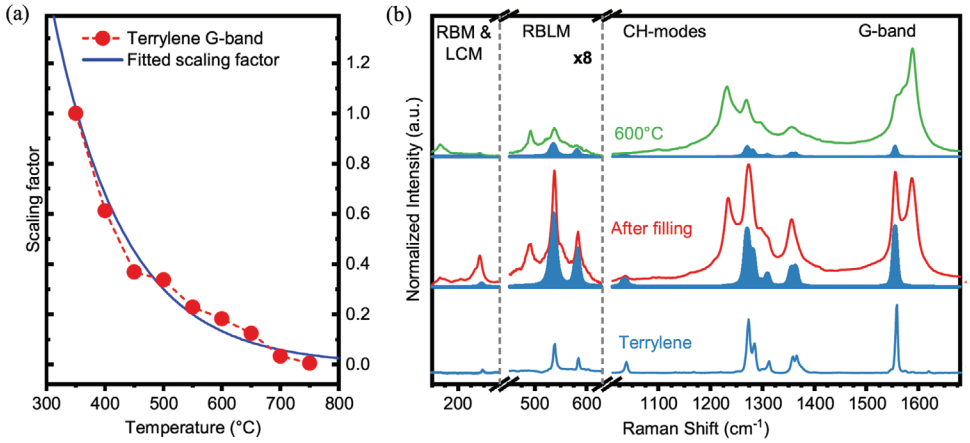

Figure 4. a) The G-band of terrylene at 1555 cm^{-1} was extrapolated from the experimental spectra by a Voigtian fit over a linear baseline. The peak's intensity is shown for all annealing temperatures completing an evolution as a function of temperature. The exponential fit is used later as scaling factor in (b). b) Empirical model for the subtraction of terrylene spectral contribution based on the experimental crystalline terrylene spectrum recorded with a 785 nm excitation wavelength. To obtain the "terrylene signal-free" spectrum recorded with 633 nm, the scaling factor defined in (a) is used. This exemplifies the process shown for samples right after filling and when annealed at 600 °C .

the GNR. On the other hand, the D-band, usually observed for SWCNT at ≈1300 cm^{-1}, is not clearly discernible in the spectra of the filled hybrids. This is partly because of an overlap with the CH-modes, which appear at lower frequencies on the spectra corresponding to the hybrids compared to those measured in clean terrylene, where they appear only above 1200 cm^{-1}. The position of the CH-modes of the 5-AGNR@SWCNT at lower frequencies could be associated to the H-terminations on the encapsulated terrylene edges. These terminations are particularly important for defining the physical properties of the GNR and implicitly on the overall Raman signal. However, this Raman shift can also be related to the formation of the expected nanoribbons,[36,37] in which case, other strong in-plane bending $CH_{n_{GNR}}$ -modes characteristic of the 5-AGNR@SWCNT will need to be considered.

Looking closer into the region between 1200 and 1400 cm^{-1}, various peaks that originate from the CH vibrations are visible. Their relative intensities vary according to the excitation wavelength and the signal is enhanced in the vicinity of the corresponding structure's energy gap. In the spectra recorded after the SWCNTs are filled, the terrylene monomer peaks project dominantly when the 568 and 633 nm wavelengths are used, while their intensity lowers significantly when using 785 nm. The new lines appearing in the RBLM and CH-mode regions (in resonance with the 785 nm excitation wavelength), are neither related to the SWCNT nor to terrylene. They consequently correspond to the encapsulated 5-AGNR@SWCNT and the most dominant of these is found at 1230 cm^{-1}. Given that the spectrum from the 633 nm excitation exhibits a better resolved fine structure in the CH-mode region, a peak deconvolution was done by a Voigtian fit as shown in Figure 3b. The peak centers of the identified components labeled from 1 to 8 are listed in the table of Figure 3c. Most of the peaks found can be related to known terrylene CH-vibrations or to the SWCNT D-band. However, the highlighted peaks at 1230 and 1247 cm^{-1} most likely originate from the 5-AGNR@SWCNT hybrid system. Furthermore, the D-like mode (DLM) at ≈1365 cm^{-1}[31,38] and small out-of-plane CH-modes appear around ≈800 cm^{-1}.[39] Also SWCNT have a diameter-related response below ≈150 cm^{-1} known as the radial breathing mode (RBM), whereas the GNR have an analogous vibration related to their width, named the radial breathing-like mode (RBLM). These features are found between ≈150 cm^{-1} and ≈600 cm^{-1}, and lose the purely transversal character for short ribbons splitting into a RBLM- and RBLM+.[18]

Clearly, in the past, the key problem to investigate in detail the Raman fingerprints of the GNR in systems alike had been the superposition of Raman-active modes from the outer precursor molecules with those from the GNR. In our experiments, the DOC washing process allows removing the largest proportion of the signal contribution coming from the terrylene molecules that stay outside. However, the remaining traces of terrylene molecules adsorbed on the SWCNT's outer surface still need to be to cleared away to discern the origin of the different Raman active CH–vibrations so far identified.

2.2. Disentangling the GNR-Related Modes

A major challenge is to distinguish between the Raman modes of unpolymerized terrylene on the outside surface of the nanotubes and longer encapsulated 5-AGNR. A first rough approach to understanding the polymerization was running a sequence of measurements on the perylene, terrylene, and quaterrylene dyes. It was corroborated that the highest CH-modes of these molecules are at 1355, 1272, and 1251 cm^{-1} respectively, and they downshift as a function of molecular length (see Figure S5, Supporting Information). Further examination of the GNR edge related modes requires the removal of adsorbed terrylene. For this purpose, filled SWCNT samples were annealed for two hours in vacuum better than 10^{-5} mbar, each at a different temperature between 400 and 800 °C with 50 °C steps (see **Figure 4**a). We expect adsorbed terrylene to burn away at a lower temperature than the decomposition temperature of encapsulated GNR because of the protective role of the SWCNT's wall. To test how the intensity evolution of the

Table 1. The dominant CH-modes of terrylene and 5-AGNRs are listed. They were measured at the resonance laser line of terrylene at 633 nm and 5-AGNR at 785 nm. Because of symmetry breaking effects, the CH-modes of terrylene split into doublets.

	Peak Center [cm^{-1}]			
	$CH1_{GNR}$	$CH2_{GNR}$	$CH3_{GNR}$	DLM
Terrylene	1272	1299	–	1359
	1285	1313		1367
5-AGNR	1230	1266	1294	1350

spectral features originating from 5-AGNR@SWCNT differs from those of non-encapsulated terrylene, the spectral response for 5-AGNR@SWCNT was recorded using the 568, 633, and 785 nm laser lines (see Figures S7–S9, Supporting Information) as a function of the annealing temperature. Note that the G-band region in the spectra corresponding to the 5-AGNR@SWCNT clearly changes on the lower Raman frequency side, where terrylene has its highest intensity in the same range. Consequently, the Raman fingerprint of terrylene available from 785 nm (where the background is lowest, as explained before) together with the G-band's intensity were used in order to discern the Raman features of the 5-AGNR@SWCNT hybrid over those of the last traces of terrylene adsorbed outside the structures. Taking this into account, a Voigtian line shape analysis of the G-band of terrylene (at 1555 cm^{-1}[40]) from the samples treated at different temperatures was carried out (see Section S6, Supporting Information). The evolution of intensity of the terrylene G-band versus annealing temperatures is plotted in Figure 4a. The exponential decrease of the intensity observed for the G-band hints at the removal of the adsorbed terrylene with increasing temperatures. Therefore, the fitted pattern in blue can be used to further quantify the influence of the outer residual terrylene on the Raman spectra of the 5-AGNR@SWCNT. This curve can be used as scaling factor afterward to analyze the spectral figures for other excitation wavelengths taking into account the laser-line broadening, sensitivity, and resolution of the detector. Briefly, while using the Voigtian fits of the G band, the Gaussian width depends on the laser's emission line-width and on the spectrometer's resolution, while the Lorentzian width depends on the vibrational lifetime and Raman resonance. Having this in mind, it is possible to make an appropriate subtraction of the terrylene spectrum from the integrated signal of the 5-AGNR@SWCNT at a given annealing temperature. Section S8, Supporting Information describes in more detail the empirical model applied here for the terrylene subtraction.

Now, making use of this model, Figure 4b exemplifies the procedure for a sample measured right after filling and following a high temperature annealing at 600 °C. This analysis has been done using the spectra obtained with a 633 nm excitation wavelength because it is close to the optical gap of both terrylene and 5-AGNR@SWCNT. The corresponding empirical terrylene models, taking into account the laser-line broadening and the sensitivity of the detector, were subtracted from the experimental data, which provided spectra free from the terrylene fingerprint. Only in this way we have been able to disentangle—for the first time—peaks that can neither be attributed to terrylene nor to SWCNT, but they exclusively respond to vibrational modes from 5-AGNR.

The most prominent CH-vibration is the peak at 1230 cm^{-1}, which was also found in the deconvolution in Figure 3b. Furthermore, the peak at 1272 cm^{-1} is downshifted about 10 wavenumbers comparing the spectra of the sample right after filling and the one after annealing. However, subtracting the terrylene response it becomes apparent that this shift is due to the superposition of the $CH2_{GNR}$ mode of the 5-AGNR@SWCNT at 1266 cm^{-1} and a peak from terrylene at 1272 cm^{-1}. Additional 5-AGNR@SWCNT modes include the $CH4_{GNR}$ at 1294 cm^{-1}, the DLM_{GNR} at 1350 cm^{-1}, and the hybrid mode at 492 cm^{-1} in the RBLM region mentioned above. **Table 1** summarizes the CH-modes of terrylene and the 5-AGNR@SWCNT.

Once these modes were identified, to gain a better understanding of the observed responses, the Raman spectra for 5-AGNR with edges passivated with H atoms were computed. These GNR were modeled encapsulated in metallic and semiconducting SWCNTS. For example, top and side views of a molecular model of a 5-AGNR inside a SWCNT with (17,0) chirality (5-AGNR@(17,0)SWCNT) are shown in **Figure 5**a,b. Figure 5c shows the DFT calculated spectra for a 5-AGNR@(19,0)SWCNT and a 5-AGNR@(18,0)SWCNT, that have a semiconducting and a metallic SWCNT host, correspondingly. Both of these tubes are (±0.5 nm) close to the experimental mean diameter in the nanotube samples. The spectrum recorded with an excitation wavelength of 785 nm on the sample annealed at 600 °C is compared in the figure to the calculated spectra. The highest intensity signal of the 5-AGNR@(19,0) SWCNT can be associated to the G-band, followed by the CH-modes at 1298, 1280, and 1234 cm^{-1}. On the other hand, the G-band signal of the 5-AGNR@(18,0) is quenched, while the highest contributions in the region are the modes at 1280 and 1298 cm^{-1}, followed by the 1234 cm^{-1} mode. Additional modes arise in the lower frequency regions. For the 5-AGNR@(19,0) it is also observed that the RBLM at 534 cm^{-1} and the RBM at 460 cm^{-1} (corresponding to the nanotube) are weaker than the G-line. The hybrid mode between 460 and 492 cm^{-1} in the RBLM region originates from an asymmetric vibration of the encapsulating SWCNT. This second mode from the mixed nanotube-nanoribbon vibration is found at lower frequency in the computed spectrum of 5-AGNR@(19,0) compared to its counterpart.

Changes on the CHn_{GNR}-modes upon annealing: Looking again at figure 4b, it is clear that there are two peaks at 492 and 1230 cm^{-1} that have high intensity after subtraction of the terrylene signal normalized to the G-band scaling factor. Their intensity evolution was analyzed as a function of the annealing temperature and no changes were observed up to temperatures between 550 and 600 °C . The plot in **Figure 6** shows how their intensity starts decaying linearly at higher

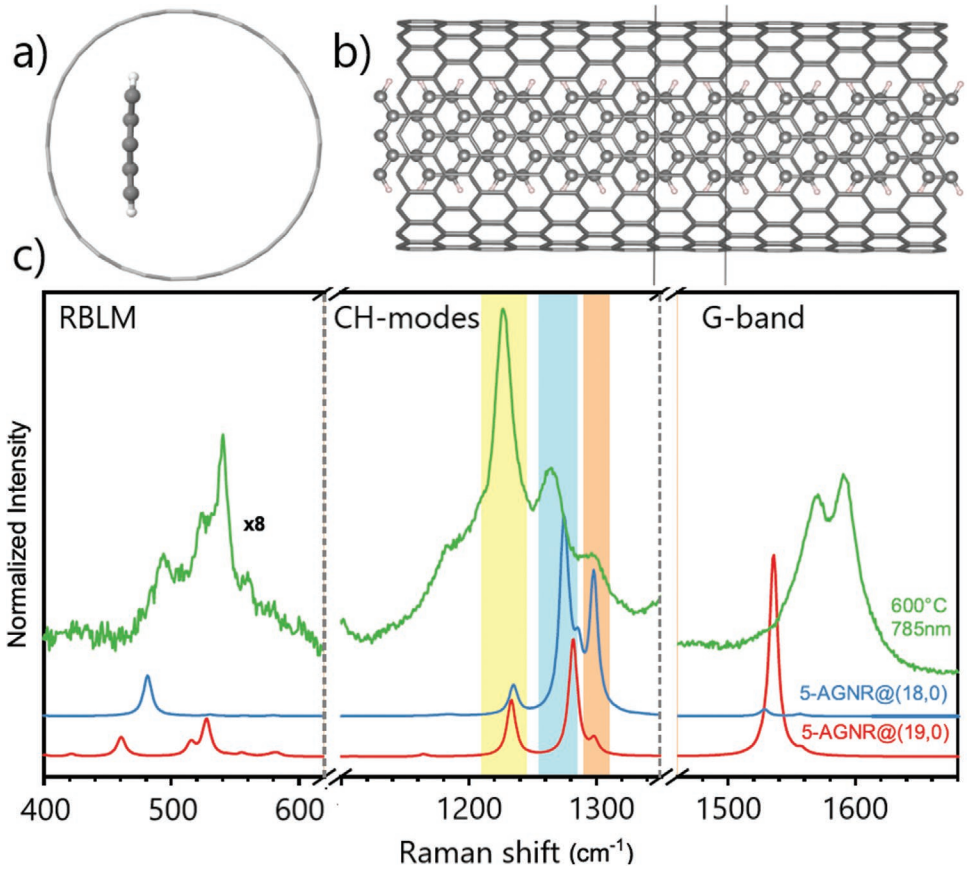

Figure 5. a) Top and b) side view of a 5-AGNR@(17,0) molecular model with edges terminated with single H atoms. The unit cell of the hybrid system is delimited by lines. c) Comparison between DFT computed spectra of 5-AGNR@(19,0) semiconducting SWCNT and 5-AGNR@(18,0) metallic SWCNT with samples of 5-AGNR@SWCNT annealed at 600 °C using a 785 nm excitation wavelength. The calculated positions of major CH vibrations are consistent with experimental data. The peaks at 1230 cm^{-1} (highlighted in yellow) and 1266 cm^{-1} (highlighted in blue) are a superposition of signals from 5-AGNR encapsulated both in metallic and semiconducting SWCNT. The largest contribution to the peak at 1294 cm^{-1} originates from 5-AGNR encapsulated in metallic SWCNT (highlighted in orange).

temperatures, which corroborates that the previous assignment of the 5-AGNR@SWCNT modes is correct. This also implies that the GNR@SWCNT hybrid structure is stable up to 550–600 °C. After this temperature, the decrease in signal-to-noise ratio points to the decomposition of GNRs inside the tubes into amorphous carbon until the thermal energy supplied is enough to form inner SWCNT.[24, 41] Taking into account the dependence of the signals in Figures 4a and 6 on temperature of the terrylene and 5-AGNR@SWCNT, it is reasonable to use data recorded from samples heated above 600 °C for further peak analysis. At this temperature threshold, the 5-AGNR signal starts to decrease, while the terrylene signal has already gone down below 20% of its original intensity. This means that applying annealing up to the described threshold defines the final conditions to keep long 5-AGNR@SWCNT before they shorten and transform into new encapsulated structures (as sketched in Figure 1e).

In summary, the CH-vibrational modes in the 5-AGNR@SWCNT hybrid system had been unraveled for the first time. Beyond the feasibility to use terrylene as a precursor molecule to make such structures, this synthesis approach represents a viable pathway to produce truly width-controlled armchair nanoribbons. A comparison with theory also allowed us to demonstrate that the edges of synthesized 5-AGNR@SWCNT are terminated with one H atom, which is consistent with the expected outcome of terrylene polymerization.

3. Conclusions

It is shown here how, compared to other dyes, terrylene can be encapsulated inside 1.4 nm diameter SWCNT and keep an optimal alignment so that it can subsequently be transformed into long 5-AGNR@SWCNT that are hydrogen passivated. No preceding studies had been able to identify distinctly the Raman active modes of such nanoribbons to the best of our knowledge. To achieve this here, the nature and evolution of isolated Raman modes corresponding to 5-AGNR@SWCNTs have been identified by developing a subtraction procedure of the terrylene Raman signal obtained with an excitation energy below its optical band gap. This allows working with a minimal fluorescence background and, in turn, enhancing the visibility of the CH vibrations that correspond to the hybrid encapsulated system. Moreover, this model introduces the use of scaling

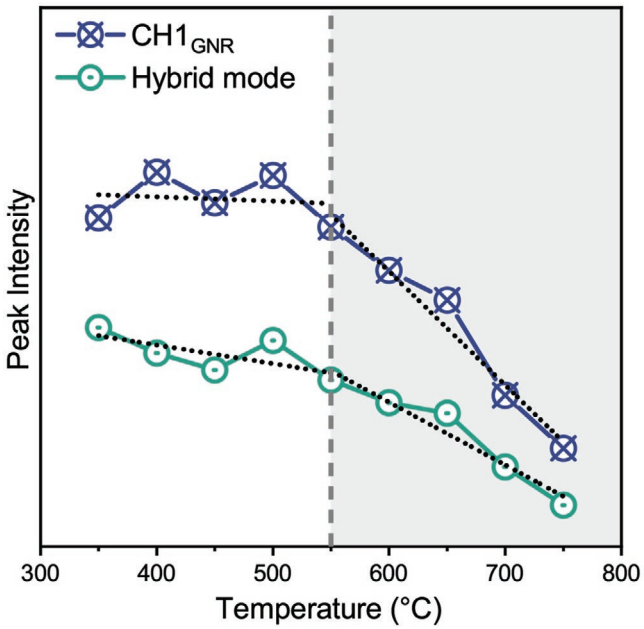

Figure 6. The $CH1_{GNR}$ mode of 5-AGNR at 1230 cm^{-1} and the hybrid mode at 492 cm^{-1} in the RBLM region were extrapolated from spectra by a Voigtian fit over a linear baseline. The spectral responses generated with an excitation wavelength of 633 nm are used here. The intensities for the $CH1_{GNR}$ mode and the hybrid mode in the RBLM region are shown. The intensities are stable up to annealing at about 550 °C . For higher annealing temperatures the signal loses intensity which hints the conversion into amorphous carbon inside SWCNT.

factors based on the G-band response, which plays a pivotal role for the future Raman characterization of GNR@SWCNT systems. For these GNR formed from terrylene as precursor, theoretical models have confirmed that the Raman signal observed for 5-AGNR@SWCNT corresponds to CH modes given by the presence of H passivating atoms.

4. Experimental Section

Materials: Arc discharge SWCNT with a mean diameter of 1.4 nm were used. Density-gradient ultracentrifugation (DGU) using sodium dodecyl sulfate (SDS) as gradient material[42] was employed to separate a fraction of semiconducting tubes with a narrow diameter distribution. The presence of ≈1% metallic SWCNT cannot be disregarded. A buckypaper was prepared and the SWCNT were opened by local heating in air at 450 °C for 30 min.[43] A 0.3 mg bucky paper and ≈2 mg of a terrylene dye were placed inside a borosilicate glass capillary closed in one end and this was connected to a high vacuum pumping system to reach an internal pressure of 10^{-7} mbar. The second end was sealed and the capillary was then kept at 350 °C for 455 h (19 days) in a tube furnace. Small terrylene van der Waals crystals as a byproduct. Therefore, to make sure that the excess terrylene material on the outside of the SWCNTs was removed, the filled bucky paper was washed multiple times with dichloromethane (DCM). Additional annealing steps were done in vacuum to analyze the sample stability and the changes in the Raman spectral features upon changes in temperature.

Raman Spectroscopy: Multifrequency Raman spectroscopy was performed with a Horiba Yobin Yvon LABRAM notch filter Raman system with a confocal microscope for the 568 and 633 nm, and at 785 nm excitation wavelengths. Additionally, a WITech alpha 300A high-resolution AFM/Raman system was used for local non-destructive characterization. The resolution of all spectra is between ≈2.5 and ≈4 cm^{-1} according to the excitation wavelength. For ease of the data analysis, all spectra were normalized to the G-band.

Calculations: Additionally, the Raman spectra for the terrylene molecule were computed with DFT at the PBE-6-31G(d,p) level augmented by a D3 dispersion term[44] with Becke– Johnson damping[44] with Gaussian 09[45] and CRYSTAL17 for molecular and 1D-periodic systems respectively.

Supporting Information

Supporting Information is available from the Wiley Online Library or from the author.

Acknowledgements

V.M. and C.B. contributed equally to this work. C.B. and V.M. acknowledge the support from the University of Vienna via the Vienna Doctoral School. V.M. and T.P. acknowledge the contribution from the Austrian Science Fund (FWF) via the research project P30431-N36. P.A. acknowledges the contribution of the COST Action CA15107 MultiComp and the COST Action EsSENce CA119, supported by the European Cooperation in Science and Technology(COST). J.L. and M.M.F. acknowledge support through the project IF/00894/2015, the advanced computing project CPCA/A2/2524/2020 granting access to the Navigator cluster at LCA-UC and within the scope of the project CICECO-Aveiro Institute of Materials, UIDB/50011/2020 & UIDP/50011/2020 funded by national funds through the Portuguese Foundation for Science and Technology I.P./MCTES. L.S. acknowledges support by the National Natural Science Foundation of China (No. 51902353), Guangdong Basic and Applied Basic Research Foundation (No. 2019A1515011227), and State Key Laboratory of Optoelectronic Materials and Technologies (No.OEMT-2021-PZ-02). K.C. thanks the support from the Shanghai "Post-Qi-Ming-Xing Plan" for Young Scientists, China (Grant No. 21QA1406300). K.Y. acknowledges the support from JST CREST Grant Number JPMJCR17I5.

Conflict of Interest

The authors declare no conflict of interest.

Data Availability Statement

The data that support the findings of this study are available in the supplementary material of this article.

Keywords

carbon nanotube hybrids, graphene nanoribbons, Raman spectroscopy, terrylene

Received: February 28, 2022
Revised: May 17, 2022
Published online:

[1] M. M. Shulaker, G. Hills, N. Patil, H. Wei, H.-Y. Chen, H.-S. P. Wong, S. Mitra, *Nature* **2013**, *501*, 526.
[2] G. Hills, C. Lau, A. Wright, S. Fuller, M. D. Bishop, T. Srimani, P. Kanhaiya, R. Ho, A. Amer, Y. Stein, D. Murphy, Arvind, A. Chandrakasan, M. M. Shulaker, *Nature* **2019**, *572*, 595.

[3] H. C. Chin, C. S. Lim, W. S. Wong, K. A. Danapalasingam, V. K. Arora, M. L. P. Tan, *J. Nanomater.* **2014**, *2014*, 879813.
[4] M. Romagnoli, V. Sorianello, M. Midrio, F. H. L. Koppens, C. Huyghebaert, D. Neumaier, P. Galli, W. Templ, A. D'Errico, A. C. Ferrari, *Nat. Rev. Mater.* **2018**, *3*, 392.
[5] A. Montanaro, W. Wei, D. D. Fazio, U. Sassi, G. Soavi, P. Aversa, A. C. Ferrari, H. Happy, P. Legagneux, E. Pallecchi, *Nat. Commun.* **2021**, *12*, 2728.
[6] P. Ruffieux, S. Wang, B. Yang, C. Sánchez-Sánchez, J. Liu, T. Dienel, L. Talirz, P. Shinde, C. A. Pignedoli, D. Passerone, T. Dumslaff, X. Feng, K. Müllen, R. Fasel, *Nature* **2016**, *531*, 489.
[7] J. P. Llinas, A. Fairbrother, G. Borin Barin, W. Shi, K. Lee, S. Wu, B. Yong Choi, R. Braganza, J. Lear, N. Kau, W. Choi, C. Chen, Z. Pedramrazi, T. Dumslaff, A. Narita, X. Feng, K. Müllen, F. Fischer, A. Zettl, P. Ruffieux, E. Yablonovitch, M. Crommie, R. Fasel, J. Bokor, *Nat. Commun.* **2017**, *8*, 633.
[8] R. B. Payod, D. Grassano, G. N. C. Santos, D. I. Levshov, O. Pulci, V. A. Saroka, *Nat. Commun.* **2020**, *11*, 82.
[9] M. Fujita, K. Wakabayashi, K. Nakada, K. Kusakabe, *J. Phys. Soc. Jpn.* **1996**, *65*, 1920.
[10] K. Nakada, M. Fujita, G. Dresselhaus, M. S. Dresselhaus, *Phys. Rev. B* **1996**, *54*, 17954.
[11] M. Kolmer, A. Steiner, I. Izydorczyk, W. Ko, M. Engelund, M. Szymonski, A.-P. Li, K. Amsharov, *Science* **2020**, eabb8880.
[12] T. Kitao, M. W. A. MacLean, K. Nakata, M. Takayanagi, M. Nagaoka, T. Uemura, *J. Am. Chem. Soc.* **2020**, *142*, 5509.
[13] H. Kuzmany, L. Shi, M. Martinati, S. Cambré, W. Wenseleers, J. Kürti, J. Koltai, G. Kukucska, K. Cao, U. Kaiser, T. Saito, T. Pichler, *Carbon* **2021**, *171*, 221.
[14] J. M. Tour, *Chem. Mater.* **2013**, *26*, 163.
[15] A. Narita, Z. Chen, Q. Chen, K. Müllen, *Chem. Sci.* **2019**, *10*, 964.
[16] H. Sakaguchi, Y. Kawagoe, Y. Hirano, T. Iruka, M. Yano, T. Nakae, *Adv. Mater.* **2014**, *26*, 4134.
[17] Z. Chen, W. Zhang, C.-A. Palma, A. L. Rizzini, B. Liu, A. Abbas, N. Richter, L. Martini, X.-Y. Wang, N. Cavani, H. Lu, N. Mishra, C. Coletti, R. Berger, F. Klappenberger, M. Kläui, A. Candini, M. Affronte, C. Zhou, V. D. Renzi, U. del Pennino, J. V. Barth, H. J. Räder, A. Narita, X. Feng, K. Müllen, *J. Am. Chem. Soc.* **2016**, *138*, 15488.
[18] J. Overbeck, G. B. Barin, C. Daniels, M. L. Perrin, O. Braun, Q. Sun, R. Darawish, M. De Luca, X.-Y. Wang, T. Dumslaff, A. Narita, K. Müllen, P. Ruffieux, V. Meunier, R. Fasel, M. Calame, *ACS Nano* **2019**, *13*, 13083.
[19] J. Overbeck, G. Borin Barin, C. Daniels, M. L. Perrin, L. Liang, O. Braun, R. Darawish, B. Burkhardt, T. Dumslaff, X.-Y. Wang, A. Narita, K. Müllen, V. Meunier, R. Fasel, M. Calame, P. Ruffieux, *Phys. Status Solidi B* **2019**, *256*, 1900343.
[20] G. Borin Barin, A. Fairbrother, L. Rotach, M. Bayle, M. Paillet, L. Liang, V. Meunier, R. Hauert, T. Dumslaff, A. Narita, K. Müllen, H. Sahabudeen, R. Berger, X. Feng, R. Fasel, P. Ruffieux, *ACS Appl. Nano Mater.* **2019**, *2*, 2184.
[21] H. Shiozawa, T. Pichler, A. Grüneis, R. Pfeiffer, H. Kuzmany, Z. Liu, K. Suenaga, H. Kataura, *Adv. Mater.* **2008**, *20*, 1443.
[22] H. Shiozawa, C. Kramberger, R. Pfeiffer, H. Kuzmany, T. Pichler, Z. Liu, K. Suenaga, H. Kataura, S. R. P. Silva, *Adv. Mater.* **2010**, *22*, 3685.
[23] X. Liu, H. Kuzmany, T. Saito, T. Pichler, *Phys. Status Solidi B* **2011**, *248*, 2492.
[24] L. Shi, P. Rohringer, K. Suenaga, Y. Niimi, J. Kotakoski, J. C. Meyer, H. Peterlik, M. Wanko, S. Cahangirov, A. Rubio, Z. J. Lapin, L. Novotny, P. Ayala, T. Pichler, *Nat. Mater.* **2016**, *15*, 634.
[25] L. Shi, K. Yanagi, K. Cao, U. Kaiser, P. Ayala, T. Pichler, *ACS Nano* **2018**, *12*, 8477.
[26] S. Heeg, L. Shi, T. Pichler, L. Novotny, *Carbon* **2018**, *139*, 581.
[27] W. Cui, L. Shi, K. Cao, U. Kaiser, T. Saito, P. Ayala, T. Pichler, *Angew. Chem., Int. Ed.* **2021**, *60*, 9897.
[28] A. Chuvilin, E. Bichoutskaia, M. C. Gimenez-Lopez, T. W. Chamberlain, G. A. Rance, N. Kuganathan, J. Biskupek, U. Kaiser, A. N. Khlobystov, *Nat. Mater.* **2011**, *10*, 687.
[29] A. V. Talyzin, I. V. Anoshkin, A. V. Krasheninnikov, R. M. Nieminen, A. G. Nasibulin, H. Jiang, E. I. Kauppinen, *Nano Lett.* **2011**, *11*, 4352.
[30] T. W. Chamberlain, J. Biskupek, G. A. Rance, A. Chuvilin, T. J. Alexander, E. Bichoutskaia, U. Kaiser, A. N. Khlobystov, *ACS Nano* **2012**, *6*, 3943.
[31] H. Kuzmany, L. Shi, J. Kürti, J. Koltai, A. Chuvilin, T. Saito, T. Pichler, *Phys. Status Solidi RRL* **2017**, *11*, 1700158.
[32] T. Koyama, K. Fujiki, Y. Nagasawa, S. Okada, K. Asaka, Y. Saito, H. Kishida, *J. Phys. Chem. C* **2018**, *122*, 5805.
[33] N. Richter, Z. Chen, A. Tries, T. Prechtl, A. Narita, K. Müllen, K. Asadi, M. Bonn, M. Kläui, *Sci. Rep.* **2020**, *10*, 1988.
[34] M. E. Abbassi, M. L. Perrin, G. B. Barin, S. Sangtarash, J. Overbeck, O. Braun, C. J. Lambert, Q. Sun, T. Prechtl, A. Narita, K. Müllen, P. Ruffieux, H. Sadeghi, R. Fasel, M. Calame, *ACS Nano* **2020**, *14*, 5754.
[35] A. Jorio, R. Saito, G. Dresselhaus, M. S. Dresselhaus, *Raman Spectroscopy in Graphene Related Systems*, Wiley-VCH, Weinheim, Germany **2011**.
[36] J. Zhou, J. Dong, *Appl. Phys. Lett.* **2007**, *91*, 173108.
[37] I. A. Verzhbitskiy, M. D. Corato, A. Ruini, E. Molinari, A. Narita, Y. Hu, M. G. Schwab, M. Bruna, D. Yoon, S. Milana, X. Feng, K. Müllen, A. C. Ferrari, C. Casiraghi, D. Prezzi, *Nano Lett.* **2016**, *16*, 3442.
[38] H. Kuzmany, L. Shi, T. Pichler, J. Kürti, J. Koltai, F. Hof, T. Saito, *Phys. Status Solidi B* **2015**, *252*, 2530.
[39] R. Gillen, M. Mohr, C. Thomsen, J. Maultzsch, *Phys. Rev. B* **2009**, *80*, 155418.
[40] M. Wojdyr, *J. Appl. Crystallogr.* **2010**, *43*, 1126.
[41] P. Rohringer, L. Shi, P. Ayala, T. Pichler, *Adv. Funct. Mater.* **2016**, *26*, 4874.
[42] K. Yanagi, T. Iitsuka, S. Fujii, H. Kataura, *J. Phys. Chem. C* **2008**, *112*, 18889.
[43] Y. Yamada, O. Kimizuka, K. Machida, S. Suematsu, K. Tamamitsu, S. Saeki, Y. Yamada, N. Yoshizawa, O. Tanaike, J. Yamashita, F. Don, K. Hata, H. Hatori, *Energy Fuels* **2010**, *24*, 3373.
[44] S. Grimme, S. Ehrlich, L. Goerigk, *J. Comput. Chem.* **2011**, *32*, 1456.
[45] M. J. Frisch, G. W. Trucks, H. B. Schlegel, G. E. Scuseria, M. A. Robb, J. R. Cheeseman, G. Scalmani, V. Barone, B. Mennucci, G. A. Petersson, H. Nakatsuji, M. Caricato, X. Li, H. P. Hratchian, A. F. Izmaylov, J. Bloino, G. Zheng, J. L. Sonnenberg, M. Hada, M. Ehara, K. Toyota, R. Fukuda, J. Hasegawa, M. Ishida, T. Nakajima, Y. Honda, O. Kitao, H. Nakai, T. Vreven, J. A. Montgomery Jr., et al., *Gaussian-09 Revision D.01*, Gaussian Inc. Wallingford CT **2009**.